Simpson Fiona (Orcid ID: 0000-0001-7589-115X)

The role of tectonic-plate thickness and mantle conductance in determining regional vulnerability to extreme space weather events: possible enhancement of magnetic source fields by secondary induction in the asthenosphere

Fiona Simpson[1] and Karsten Bahr[2]

[1] *School of Ocean and Earth Science, University of Southampton, National Oceanography Centre, European Way, SO14 3ZH, UK; f.simpson@soton.ac.uk*

[2] *Institut für Geophysik, Georg-August Universität Göttingen, Friedrich-Hund-Platz 1, Göttingen, Germany*

Corresponding author: Fiona Simpson (f.simpson@soton.ac.uk)

Key Points:

- Novel consideration of coupling between external storm-time geomagnetic fields and Earth's deep electrical conductivity structure.
- Tectonic-plate thickness and electrical conductivity of underlying asthenosphere shown to affect regional vulnerability to space weather.
- Estimated electric fields for 8th September 2017 and 30th October "Halloween" 2003 storms in central Scotland and southern Sweden.

This article has been accepted for publication and undergone full peer review but has not been through the copyediting, typesetting, pagination and proofreading process which may lead to differences between this version and the Version of Record. Please cite this article as doi: 10.1029/2020SW002587

Abstract

During magnetic storms, solar-magnetosphere-ionosphere-Earth interactions give rise to geomagnetically induced currents (GICs) in man-made technological conductors such as power grids, gas pipelines and transport networks with potentially damaging outcomes. Generally, electrically conductive regions of the Earth are assumed to be less at risk to GICs than resistive ones, since induced electric fields associated with GICs are linearly related to given magnetic source fields via Earth's impedance. Here, we show that magnetic source fields associated with storms can be enhanced by secondary electromagnetic (EM) induction in Earth's electrically conductive asthenosphere and that this previously neglected effect can give rise to larger electric fields close to the lithosphere-asthenosphere boundary in regions where the conductance of the asthenosphere is higher. Our analysis of data from the 30th October 2003 "Halloween" and 8th September 2017 storms shows that the magnitudes of electric fields from both storms are affected by lithospheric plate thickness and asthenosphere conductance (conductivity-thickness product) and that they are 5 times larger in southern Sweden (> 5 V/km for the 30th October 2003 "Halloween" storm) than in central Scotland. Our results provide insight into why Sweden experienced a storm-related power outage in 2003, whereas Scotland didn't.

Plain Language Summary

Space weather is generated by changes in the rate at which the Sun emits high-velocity, charged particles (plasma) that are collectively referred to as the "solar wind". Just as extreme atmospheric perturbations cause meteorological storms whose high-velocity winds can damage ground-based infrastructure, extreme electromagnetic perturbations of Earth's magnetosphere and ionosphere due to fluctuations in solar-wind pressure cause magnetic storms that drive hazardous, quasi-DC currents through ground-based linear conductors – power networks, gas pipelines and railways. These quasi-DC currents, referred to as "geomagnetically induced currents" or "GICs" can trip electricity transformers, corrode gas pipelines and cause railway signal failure. GIC hazards depend not only on external factors, but also on the Earth itself, because the external magnetic source fields interact with Earth's deep electrical conductivity – i.e., electric fields that drive surficial GICs are induced deeper within the Earth. Here, we investigate how the regionally-variable thickness of Earth's quasi-rigid outer, electrically-resistive shell – the "tectonic plate" or "lithosphere" – and region-dependent conductance of the underlying electrically conductive layer known as the "asthenosphere" modify surface electric fields making some regions of the world inherently more vulnerable to extreme space weather events than others.

1 Introduction

Magnetic storms occur when high-velocity plasma from solar flares or coronal mass ejections (CMEs) interacts with Earth's magnetosphere (Chapman and Ferraro, 1931). During the main phase of magnetic storms, ring-currents (Daglis et al., 1999) located tens of thousands of kilometers above Earth's surface generate magnetic fields that induce electric fields in Earth at depths depending on their wavelengths and Earth's conductivity structure (e.g., Simpson and Bahr, 2005). These electric fields generate potentially hazardous geomagnetically induced currents (GICs) in large-scale technological infrastructure such as power distribution networks (e.g., Bolduc, 2002; Wik et al., 2009; Radasky, 2011; Cannon et al., 2013). Whereas geomagnetic field variations have been continuously recorded at observatories around the world for over a century, there is a paucity of measurements of electric fields induced during magnetic storms in many regions of the industrialised world. Therefore, our

direct knowledge of these enhanced fields, their interaction with Earth's conductivity structure and our ability to model the hazard they pose is limited.

Magnetotellurics (MT) is a passive electromagnetic technique that harnesses natural fluctuations in the electric and magnetic fields induced in Earth due to solar-magnetosphere-ionosphere interactions to study the electrical conductivity of Earth's crust and mantle (e.g., Simpson and Bahr, 2005). By sampling these electric and magnetic fields simultaneously at a fixed sample rate, a quasi-continuous time series is recorded, which can be decomposed into its constituent electric and magnetic spectra at discrete frequencies via Fourier transform. Cross-correlation of these spectra for each frequency then allows computation of a frequency- and direction-dependent impedance tensor, **Z** (Cagniard, 1953; Simpson and Bahr, 2005):

$$\begin{pmatrix} E_x \\ E_y \end{pmatrix} = \begin{pmatrix} Z_{xx} & Z_{xy} \\ Z_{yx} & Z_{yy} \end{pmatrix} \begin{pmatrix} B_x / \mu_o \\ B_y / \mu_o \end{pmatrix} \qquad (1)$$

Where $\boldsymbol{E}$ is electric field, $\boldsymbol{H} = \boldsymbol{B}/\mu_0$ is magnetic field, subscripts x and y denote north-south and east-west orientated fields, respectively and μ_0 is the permeability of free space. For stable, tectonic environments these impedances can be considered stationary (e.g., Hanekop and Simpson, 2006). Impedances can also be obtained from electrical conductivity models. With perfectly sampled data that is well fitted by a model, measured and modelled impedances should converge. However, perfectly sampled data are rarely available. In the real world there are always differences between modelled and measured impedances. Simpson and Bahr (2020a, 2020b) point out that for space weather applications the conductivity structure under an MT site is better described by a measured impedance tensor than by any conductivity model that was derived from such measured impedances, where some form of error propagation and data misfit criteria are applied.

Equation (1) suggests a way of approximating the electric fields at a site where only the geomagnetic fields have been recorded during a magnetic storm if an MT impedance tensor is available for that site (Kelbert et al., 2017; Simpson and Bahr, 2020a). Equation (1) is only strictly valid for the case of plane-wave (i.e., uniform) exciting fields far above Earth's surface. The primary driver of the main phase of magnetic storms is a ring-current lying in the equatorial plane, 3-8 Earth radii above Earth's surface (Daglis, 1999) and this can be treated as a quasi-uniform source. However, departures from the plane-wave assumption occur at high latitudes during storms due to ionospheric currents associated with the auroral electrojet located 100-150 km above Earth's surface. For ring-current models of magnetic storms, we expect the B_x and E_y components to evince the largest variations. Time derivatives of magnetic time series recorded during the 30th October "Halloween" magnetic storm in Sweden are strongly north-south polarised, supporting the assumption of approximately east-west oriented induced electric fields for this storm (Watermann and Gleisner, 2009). During times of strong westward electrojets, large GICs are common in Scandinavia (Viljanen et al., 2001) and the 30th October 2003 "Halloween" magnetic storm caused a blackout in Malmö, Sweden. Wik et al. (2009) have calculated that GICs of up to 330 A may have flowed in the Swedish power network a few minutes before the Malmö blackout, whilst GICs of 42 A were recorded in the power grid at Strathaven, Scotland (Thomson et al., 2005) during the same event. These point estimates depend on the transmission-line voltages associated with induced electric fields encompassing the entire network.

Electromagnetic fields are dispersive. Therefore, the magnitudes of GIC-driving electric fields witnessed at the surface of the Earth depend not only on characteristics of the external storm-time magnetic field, but also on the electrical conductivity structure deep within the Earth, where component frequencies of these surface electric fields are induced. In August 2017, we deployed 7 magnetotelluric (MT) instruments in Scotland to (i) monitor electric and magnetic fields and (ii) investigate regional conductivity structure. These instruments registered the 8th September 2017 magnetic storm (Simpson and Bahr, 2020a), the largest magnetic storm since the 30th October 2003 "Halloween" storm. Here, we compare electromagnetic data from the 8th September 2017 and 30th October "Halloween" magnetic storms in Scotland and Sweden, differences in the region-dependent thickness of the Earth's quasi-rigid outer, electrically-resistive shell known as the "tectonic plate" or "lithosphere" and the region-dependent conductance of the underlying electrically conductive layer known as the "asthenosphere" to demonstrate the importance of coupling between electromagnetic fields external and internal to the Earth in generating GICs.

2 Methods

2.1 Internal and external parts of the geomagnetic field

The horizontal magnetic field, B_h and internally induced magnetic field B_i are related to the external source field B_e via conductance, τ, according to (c.f. A2.19 in Simpson and Bahr 2005):

$$B_h = B_e + B_i = B_e(1 + \tau/\tau_0) \qquad (2)$$

Where τ_0 is the mantle conductance for the extreme case in which the internal part of the magnetic field is as large as the external source field. Hence, for $\tau = \tau_0$, electromagnetic induction in the Earth increases the horizontal magnetic field observed at the surface by a factor of 2 relative to the external source field, whereas $\tau > \tau_0$ leads to horizontal magnetic fields that are more than twice the external magnetic source field and vice versa for $\tau < \tau_0$. Therefore, for regional studies of the hazard associated with geomagnetic storms, convolution of the geomagnetic fields from distant observatories with local impedance tensors may not provide correct estimates of electric field amplitudes across a region.

2.2 Frequency dependence of inductive scale length

MT impedances (Equation 1) are directly related to subterranean electrical conductivities. The tensor in Equation 1 is frequency-dependent. Therefore, it contains information about the depth to which electromagnetic fields penetrate. This penetration depth can be expressed in terms of the complex inductance scale length tensor, $\boldsymbol{C}$, which for the simplistic case of a homogeneous half-space is defined as (Weidelt, 1972; Schmucker, 1973):

$$\boldsymbol{C} = p/2 - \mathrm{i}\,p/2 = \frac{\boldsymbol{Z}}{\mathrm{i}\omega} \qquad (3)$$

Where $p = \sqrt{2/\mu_0\sigma\omega}$ is the electromagnetic skin depth and μ_0 is magnetic permeability of free space, σ is the conductivity of the medium penetrated and ω is angular frequency. A qualitative interpretation of Equation 3 is that penetration depth increases as electromagnetic wave period increases (i.e. as frequency decreases) and that the depths imaged by different sounding periods will depend on the conductivity structure, with electromagnetic waves of a given period being less attenuated and therefore reaching greater depths in resistive

environments than in more conductive ones. Hence, the Earth acts as a filter that modifies the electromagnetic fields induced within it by external magnetovariational fields.

2.3 Dependence of electric fields on conductance and inductive scale length

For a 3-layer medium comprised of a resistive lithosphere of thickness *h*, a conductive asthenosphere of conductance τ such that $\omega\mu_0\tau p \gg 1$ and an underlying moderately conductive (100 Ωm) upper mantle layer in which electromagnetic fields with angular frequency ω have a penetration depth *p*, the inductance scale length given in Equation 3 is modified (Bahr et al., 2000):

$$C \approx h - \mathrm{i}j \tag{4}$$

Where $j = \omega\mu_0\tau$. Therefore, from equations 1-4, the horizontal electric field, E_h, is given by:

$$E_\mathrm{h} = i\omega C B_\mathrm{h} = \mathrm{i}\omega B_\mathrm{e}\left(h + \frac{\tau}{j\tau_0} + \mathrm{i}\left[\frac{h\tau}{\tau_0} - \frac{1}{j}\right]\right) \tag{5}$$

And, the modulus of E_h is given by:

$$|E_h| = \omega B_\mathrm{e}\sqrt{\left(h^2 + \frac{1}{\omega^2{\mu_0}^2\tau^2}\right)\left(1 + \left[\frac{\tau}{\tau_0}\right]^2\right)} \tag{6}$$

This expression for the magnitude of the horizontal electric field contains competing terms with regard to the effect of conductance, with larger conductance promoting larger magnetic fields that increase $|E_h|$ on the one hand and smaller inductance scale lengths that decrease $|E_h|$ on the other. For a given lithospheric thickness, for all reasonable values of τ_0, the τ-term in the second bracket has a larger effect on $|E_h|$ than the τ-term in the first bracket. For the case of plane-wave electromagnetic source fields, equation (1) embodies the principle that as the thickness of the resistive lithosphere increases, the electric fields induced in it also increase as well as the principle that as the conductance of the asthenosphere increases, induced electric fields with sufficiently long periods to penetrate into the asthenosphere are attenuated. However, storm-time magnetic source fields are not plane wave. In this case, equation 6 suggests that there is a period range corresponding to penetration depths immediately below the lithosphere-asthenosphere boundary (LAB) in which enhancement of magnetic fields within the conductive asthenosphere could cause electric fields to be increased rather than decreased.

2.4 Estimation of asthenosphere conductance

For a 3-layer medium comprised of a resistive lithosphere of thickness *h*, a conductive asthenosphere of conductance τ and an underlying moderately conductive (100 Ωm) upper mantle layer in which electromagnetic fields with angular frequency ω have a penetration depth *p*, Wait's recursion formula (Wait, 1954) for the Schmucker-Weidelt transfer function, $C(\omega)$, (Weidelt, 1972; Schmucker, 1973) reduces to (c.f. Simpson and Bahr 2005, equation 2.44):

$$C = \frac{p/2 - ip/2 + h}{1 + i\omega\mu_0\tau(p/2 - ip/2)} \tag{7}$$

It has further been shown by Bahr et al. (2000) that the real (Re) and imaginary(Im) parts of $C(\omega)$ can be expressed as polynomials in $\omega\mu_0\tau p$ and that for large asthenosphere conductance, τ, such that $\omega\mu_0\tau p \gg 1$ and long periods such that $\mathrm{Re}(C) > h$, the MT phase, ϕ, tends to 90° and is related to τ via:

$$\tan(\emptyset) = -\frac{\mathrm{Re}(C)}{\mathrm{Im}(C)} = \omega\mu_0\tau h \quad (8)$$

3 Results

3.1 Comparison of measured magnetic fields in Scotland and Sweden during magnetic storms

For the 8th September 2017 storm, the amplitude of B_x, which induces orthogonally-oriented (E_y) electric fields, is 1.75 times as large at UPS geomagnetic observatory, Sweden compared to RAN, an MT site in central Scotland (Figure 1a). A similar enhancement occurs for the 30th October 2003 "Halloween" storm, comparing data from UPS (Sweden) and ESK (Scotland) geomagnetic observatories (Figure 1b). As the latitudes of these two sites differ by only 3°, we would not expect such large differences in magnetic field amplitudes to be generated by the external geometry of the storm source field alone. Further arguments against the observed differences being attributable to source field geometry and heterogeneity are provided in Section 3.3.

3.2 Estimated electric fields for the 8th September 2017 and 30th October "Halloween" magnetic storms in Scotland and Sweden

A good agreement between the measured electric fields and those calculated by multiplying measured magnetic field spectra with frequency-dependent impedance tensors computed from time series obtained before and after the 8th September 2017 storm has been demonstrated previously (Simpson and Bahr, 2020a). This agreement between measured and estimated electric fields – typified by site RAN, Scotland (Figure 2) – justifies more general application of this technique for nowcasting electric fields to investigate storm-related hazards.

Figure 2 also shows electric fields computed using geomagnetic observatory data from UPS, Sweden for the same 7th-8th September 2017 time interval and a local impedance tensor obtained from the BEAR array (Bahr and Simpson, 2002). E_y fields are 5 times bigger for the Swedish site compared to the Scottish site, reaching peak-to-peak amplitudes of 1.25 V/km at UPS compared to 0.25 V/km at RAN. We similarly computed electric fields for the 30th October 2003 "Halloween" storm near UPS and ESK observatories (Figure 3). At UPS, peak-to-peak electric field variations of 5.6 V/km may have occurred, whereas at ESK, induced voltages were likely less than those witnessed at UPS during the smaller 8th September 2017 storm (Figure 2). Hence, the region around UPS, Sweden appears to be more vulnerable to extreme space weather events than Scotland. This is consistent with the observation that large GICs are common in Scandinavia (Viljanen et al., 2001).

3.3 Source field geometry

Whereas for the estimation of the electrical impedance from MT data, a plane-wave source (with zero wavenumber, $\boldsymbol{k}$) is assumed, a magnetic storm is not a homogenous source and

therefore the diffusion equation that describes the induction process applicable to MT is replaced by:

$$\frac{\mathrm{d}^2}{\mathrm{d}z^2}F(z,\boldsymbol{k},\omega) = (|\boldsymbol{k}|^2 + i\omega\mu_0\tau)F(z,\boldsymbol{k},\omega) \quad (9)$$

The source heterogeneity is best understood for the solar-quiet magnetic daily variation (Sq) generated by current vortices within the ionosphere, with a wavenumber for the m'th Sq harmonic (Bahr and Filloux, 1989):

$$\boldsymbol{k} = \frac{[(m+2)(m+1)\sin\theta]}{mR} \quad (10)$$

Where θ is the co-latitude and R is the Earth's radius. For the first and second harmonics, the corresponding wavelength $\lambda = 2\pi/\boldsymbol{k} = 9000$ km, which is roughly the diameter of the Sq vortex. This wavelength is greater than a factor 10 larger than the penetration depth at the associated frequencies, but is nevertheless sufficiently small to justify the need for a description of the source-field geometry for the case of Sq variations. In contrast, a geomagnetic storm modelled with a ring current having a radius of between 3-8 Earth radii (Daglis, 1999) is described by wavelengths significantly larger than the penetration depths reached in MT studies. Indeed, Osipova et al. (1989) have shown that for Scandinavia, electromagnetic source field heterogeneities only play a more significant role than conductivity structure at periods longer than 10 000 s. Therefore, for magnetic storms (in contrast to Sq studies), the source geometry should not play a major role at the MT sounding periods considered in our study. A caveat to this is that we cannot entirely exclude the possibility that substorms associated with much smaller current systems in the ionosphere occur during any particular geomagnetic storm. However, for the 8th September 2017 storm, source field heterogeneities associated with substorms cannot be significant for two reasons: i) Other sites running simultaneously with RAN during the 8th September 2017 storm >100 km away, show very similar magnetovariations and the remaining differences are partly due to horizontal gradients in mantle conductivity as indicated by small, but non-vanishing magnetic perturbation tensors (Schmucker, 1970), $\boldsymbol{W}$ (Simpson and Bahr, 2020a); ii) Our comparison between the electric fields measured during the 8th September storm and those predicted by use of the MT impedances (Figure 2) offers a way of quantifying the errors introduced by any source field heterogeneities: since the effect of the 3D conductivity distribution on the electric field at a site is completely described by the frequency-dependent impedance tensors and since these impedance tensors are derived assuming a plane-wave source, any discrepancies between the measured and estimated electric fields at a particular site can only be attributable to departures from the plane-wave source ensuing from either the magnetic storm or other sources of noise that are filtered out during MT data processing (Egbert and Booker, 1986). Figure 2 demonstrates, however, that our technique of estimating the electric fields during the storm using MT impedances generates field amplitudes similar to those measured during the storm – i.e., source field heterogeneities are negligible and the plane wave assumption appears approximately valid. Scaling between observed and estimated electric fields for the 8th September 2017 storm has been rigorously investigated by Simpson and Bahr (2020a), who showed that discrepancies are likely to be attributable to source-field polarisation.

3.4 Mantle conductance

Amplitude spectra for the 8th September 2017 (Figure 4a, b) and 30th October 2003 "Halloween" storms (Figure 4c, d) are largest for frequencies < 0.001 Hz, or equivalently periods longer than 1000 s. These long-period signals have penetration depths (see Equation 3, Methods) deeper than the electrical LAB (Simpson, 2013) under Sweden (180 km; Bahr and Simpson, 2002) and Scotland (80 km). Cherevatova et al. (2014) have estimated from MT data with periods < 1000 s that the electrical lithosphere under the mountainous region of Southern Norway is thicker than under Sweden, as one would expect from isostatic principles. The premise that deeply-penetrating electromagnetic fields have a major influence on GICs measured at Earth's surface is further supported by large amplitude GICs in the frequency band 10^{-2} to 10^{-4} Hz corresponding to penetration depths from the lower crust to the asthenosphere measured directly in the electric power grid in Guangdong, China (Liu et al., 2008).

To date, studies of storm-related surface electric fields for the UK (Beamish et al., 2002; Ivannikova et al., 2018) have been limited to thin-sheet conductance models that only take into account the galvanic effects of ocean bathymetry and near-surface (uppermost 5 km) conductance contrasts inferred from lithology, which is known to be an unreliable indicator of conductivity. These models do not consider first-order effects of induction in the mantle (e.g., Simpson, 2002). Rosenqvist and Hall (2019) have presented a pseudo-3D conductance model for the crustal electrical conductivity structure of Sweden obtained by amalgamating and extrapolating 1D and 2D models (Rasmussen, 1987; Korja et al., 2002; Engels, 2002; Ádám, 2012). They excited their model with a spatially uniform magnetic source field and used it to infer a first-order influence of the geomagnetic coast effect (Lines and Jones, 1973; Parkinson and Jones, 1979) on the induced electric fields that drive GICs. However, the long-period electromagnetic response of surficial conductance sheets is strongly influenced by the choice of underlying electrical resistivity (Simpson, 2002). Below the crust, Rosenqvist and Hall's (2019) model contains a 1000 Ωm half-space extending to infinity. However, MT studies (e.g., Simpson, 2002; Bahr and Simpson, 2002) have demonstrated that the electrical resistivity of the continental mantle below Europe and Fennoscandia is significantly less than 1000 Ωm. The assumption of an unrealistically resistive mantle exaggerates both the coast effect and the magnitudes of the induced electric fields. Both Sweden and Scotland are surrounded by shallow, marginal seas that lie mainly on the European continental shelf rather than by deep oceans. Simpson and Bahr (2020a) have used 3D modelling (Siripunvaraporn et al., 2005) to demonstrate that the coast effect is minimal for sites in central Scotland, whereas the electrical resistivity of the underlying mantle exerts a first-order influence on the induced electric fields. This point can be further understood when we consider that MT resolves conductance – conductivity of a layer multiplied by thickness of a layer. MT studies (e.g., Haak and Hutton, 1986; Simpson et al., 1997; Simpson, 1999; Simpson, 2000; Sakkas et al., 2002; Kelbert et al., 2012) have revealed variations in the electrical conductivity of the continental crust and mantle spanning 8 orders of magnitude that in some cases affect electromagnetic transfer functions more strongly than the coast effect. A 1-Ωm, lower-crustal conductor extending throughout a 15-km thick lower crust gives a conductance contrast of 15 000 S compared to a resistive (1000-Ωm) lower-crustal layer. This is equivalent to the conductance of a 3750-m deep ocean. A 10-Ωm sub-lithospheric upper mantle extending from a depth of 180 km to the mid-mantle transition zone at 410 km (where the electrical conductivity again increases (e.g., Bahr et al., 1993) gives a conductance contrast of ca. 23 000 S, which will have a significantly greater effect on the long-period electromagnetic response than the shallow seas surrounding the UK and Sweden. We further note that long-period (> 1000 s; Figure 4) induced electric fields would have penetration depths extending

into the lower mantle according to Rosenqvist and Hall's (2019) model and this is known to be incorrect (Simpson, 2002; Simpson and Bahr, 2005).

We employ a generic Earth model with two subsurface parameters that effect MT impedances through their effects on electromagnetic fields – lithosphere thickness and asthenosphere conductance – to explain how regional differences to space weather vulnerability occur. We note that tectonic boundaries also affect induced electric fields that drive GICs in technological conductors (e.g., Dong et al., 2015). Therefore, we do not advocate using this model for estimating electric fields, but only for elucidating the processes involved. We have already demonstrated (Figure 2) that electric fields can be satisfactorily estimated by multiplying MT impedances with measured magnetic field spectra in the frequency domain. The information content of the impedances that are estimated from direct measurements of electric and magnetic fields is always greater than that of any secondary model – even one with a greater complexity than our generic model – or than impedances generated from such a model. Whilst 3D conductivity models are important in the context of investigating tectonic structure (e.g., Simpson and Warner, 1998; Simpson, 2000), they become obsolete for the purpose of estimating storm-time electric fields where MT impedances – to which all information about the effect of Earth's heterogeneous conductivity structure on electric fields are intrinsic – are available for "Models can be confirmed by the demonstration of agreement between observation and prediction, but confirmation is inherently partial" (Oreskes et al., 1994).

The asthenosphere below Scandinavia has been inferred to be electrically anisotropic (Bahr and Simpson, 2002). Therefore, three variables are required to describe its conductance (e.g., Simpson, 2013) – the magnitude and strike direction of the higher conductance and the anisotropy ratio. However, these information are entirely contained within the MT impedances used to estimate the electric fields.

At sites in Finland, the asthenosphere is electrically anisotropic with conductances of 32000 S in the SSW-NNE strike direction (Bahr, 1988) compared to 7000 S in the cross-strike direction (Bahr and Simpson, 2002). We repeated the conductance estimation technique (Bahr and Simpson, 2002; Bahr et al., 2000; Methods, section 2.4) and strike determination (Bahr, 1988) for three MT sites B09, B11 and B13 (Bahr and Simpson, 2002) close to UPS and for RAN, ESK and SEB, MT site in central Scotland (Simpson and Bahr, 2020b). Our analysis reveals that the along-strike (defined as the direction of high conductivity in an anisotropic or 2D environment) conductance of the asthenosphere under Central Sweden – 13000 S – is 3-4 times higher than under Central Scotland – 4000 S striking NW-SE at ESK to approximately E-W at RAN, whilst both regions have similar, but less well-constrained, cross-strike conductances of ca. 200 S. These strike directions are not consistent with the alignment of the coastlines, indicating that Earth's deep electrical conductivity structure rather than the coast effect dominates the long-period response functions. From Equation 1 larger electric fields correspond to higher impedances (i.e. more resistive environments) and larger magnetic fields. From equation 1, we might therefore expect the electric fields to be smaller for sites in Sweden compared to those in Scotland. However, this is only the case for E_x-polarised fields (Figures 2 and 3). Examining the time series and spectra shown in Figures 1-3, we find that the B_x, B_y and E_y fields for Sweden are larger than those for Scotland. We will next demonstrate that amplification of the magnetic fields occurs due to electromagnetic induction in Earth's asthenosphere.

3.5 Coupling between magnetic source fields and mantle conductivity

As well as a dominant external part, the time-varying component of Earth's magnetic field has a significant internal part attributable to electromagnetic induction in the Earth (Schuster, 1889). The Gauss separation (Gauss, 1839; Backus et al., 1996) enables geomagnetic fields to be decomposed into components that arise due to processes internal and external to the Earth, respectively. This decomposition is facilitated by the fact that whereas internal and external parts of B_x and B_y have the same sign, internal and external parts of B_z have different signs (Simpson and Bahr, 2005). Therefore, the measured B_z, which is the sum of external and internal vertical fields, is generally smaller than the measured horizontal components.

For plane waves impinging on a 1D Earth, B_z would be zero, but magnetic storms do not have a plane-wave source field geometry. During the 2003 and 2017 storms, B_z is significantly larger at UPS than at ESK (Figure 1). We, therefore, infer that the high mantle conductance under Sweden gives rise to a larger internal part of the magnetic field at UPS compared to ESK and RAN (see also Section 2.1, Methods). For horizontal magnetic fields at UPS, this amplification effect is significantly stronger in B_x than B_y due to the SSW-NNE orientation of the maximum conductance. According to Equation 2 (Section 2.1, Methods), these inductive effects, which are also manifest in the regional variability of horizontal magnetic transfer functions for Sweden (Bahr and Simpson, 2002) lead to the approximate doubling of the magnitude of the B_x component for Sweden compared to Scotland seen in Figure 1 for both the 8th September 2017 and 30th October 2003 "Halloween" magnetic storms.

3.6 Effect of LAB depth and conductivity on vulnerability to storms

We substituted values for lithospheric thickness and asthenospheric conductance for Sweden and Scotland, into an expression for electric field magnitude that includes amplification of magnetic fields by internal induction (Equation 6, Section 2.3, Methods) to investigate how the LAB region effects the magnitude of electric fields observed at Earth's surface. At periods of ~200 s, we find that electric fields are enhanced by both increased asthenospheric conductance and increased lithospheric thickness (Figure 5a), indicating that the effects of secondary inductance are important. At periods > 1000 s, electric fields decrease as asthenospheric conductance increases and increase as lithospheric thickness increases, indicating that lithospheric thickness exerts a primary control on electric field magnitudes (Figure 5b). Disregarding, other factors such as source field heterogeneity, our 1-D model predicts that E_y electric fields during geomagnetic storms should be approximately 2-3 times larger at UPS compared to ESK. This is in qualitatively good agreement with the average trend evident in the E_y electric-field spectra (Figure 4), given differences in the directions of maximum conductance in the electrically anisotropic asthenosphere.

4 Discussion and Conclusions

We have used MT data recorded in Scotland during the 8th September 2017 storm and geomagnetic observatory data from Sweden and Scotland recorded during the 8th September 2017 and 30th October 2003 "Halloween" storms to demonstrate that the impact of extreme space weather events cannot be adequately modelled without considering electromagnetic induction in Earth's mantle. The MT impedances that we have used to estimate electric fields are more complete than any model as they contain within them all information regarding the combined effects of ocean bathymetry, mantle heterogeneity, galvanic effects and electrical anisotropy.

Our results show that the amplitude of E_y was approximately 5 times larger for UPS, Sweden compared to RAN and ESK, Central Scotland for both storms. We attribute this result to the combined effects of i) the greater thickness of the Swedish lithosphere compared to the Scottish lithosphere; ii) enhancement of the magnetic source fields as a consequence of secondary electromagnetic induction related to the higher conductance of the asthenosphere below Fennoscandia compared to Central Scotland. In March 1989, a geomagnetic storm caused a blackout in Québec, Canada (Bolduc, 2002). Lying on the North American craton, Québec like Sweden, is an area of thickened lithosphere (Jaupart et al., 1998).

Although our model is simplistic and used only to elucidate the processes involved, our results are significant because the effects of secondary induction in Earth's asthenosphere and lithospheric plate thickness have not previously been considered when compiling hazard maps (e.g., Love et al., 2016; Lucas et al., 2020) showing the electric fields likely to be associated with magnetic storms. We have demonstrated that for periods < 1000 s, corresponding to depths just below the LAB, which is at least 100 km deeper below Sweden than Scotland, a trade-off occurs between the amplification effect of high mantle conductance on the magnetic fields measured at Earth's surface and the attenuation effect of high mantle conductance on a given magnetic field. Therefore, secondary induction could be a source of error in space weather forecasting and GIC studies that concentrate on short period electromagnetic fields with shallow penetration depths do not adequately constrain the problem.

The electrical properties of the lithosphere and asthenosphere are not currently well-constrained for many parts of the world. Our paper demonstrates the existence of a practical application for this knowledge and the need for more MT data acquisition programmes similar to Earthscope in the US (e.g., Schultz, 2009; Yang et al. 2015). Upper crustal electrical conductivity models underlain by unrealistic deep crustal and mantle resistivities are inadequate for the purpose of calculating storm-time electric fields that drive GICs.

Acknowledgments and Data

This work was supported by the Natural Environment Research Council (NERC Grant NE/P016782/1. In addition to MT data collected by the authors, the results presented in this paper rely on geomagnetic data collected at ESK and UPS observatories. We thank the British Geological Survey (BGS) and Geological Survey of Sweden (SGU) for supporting their operation and INTERMAGNET for promoting high standards of magnetic observatory practice. Additionally, we thank Forestry Commission Scotland for allowing us to install MT instrumentation at RAN. We also thank Denghai Bai and an anonymous reviewer for thoughtful reviews that helped us to improve an earlier version of our manuscript.

All data discussed in this paper are presented in the Figures. Geomagnetic observatory data are available from INTERMAGNET. MT data collected by the authors will be made available digitally through the National Geoscience Data Centre (NGDC), UK prior to publication.

References

Ádám, A., Prácser, E. and Wesztergom, V. (2012). Estimation of the electric resistivity distribution (EURHOM) in the European lithosphere in the frame of the EURISGICWP2

project. *Acta Geodaetica et Geophysica Hungarica*, *47*, 377–387, https://doi.org/10.1556/AGeod.47.2012.4.1.
Backus, G., Parker R. and Constable, C. (1996). *Foundations of Geomagnetism*. Cambridge University Press, Cambridge, UK, pp. 370, ISBN: 9780521410069.
Bahr, K. (1988). Interpretation of the magnetotelluric impedance tensor: regional induction and local telluric distortion. *J. Geophys.*, *62*, 119-127, https://geophysicsjournal.com/article/129.
Bahr, K. and Filloux, J. H. (1989). Local Sq response functions from EMSLAB data. *J. Geophys. Res.*, *94*, 14 195-14 200, https://doi.org/10.1029/JB094iB10p14195.
Bahr, K., Olsen, N. and Shankland, T. J. (1993). On the combination of the magnetotelluric and the geomagnetic depth sounding method for resolving an electrical conductivity increase at 400 km depth. *Geophys. Res. Lett.*, *20*, 2937-2940, https://doi.org/10.1029/93GL02134.
Bahr, K., Bantin, M., Jantos, C., Schneider, E. and Storz, W. (2000). Electrical anisotropy from electromagnetic array data: implications for the conduction mechanism and for distortion at long periods. *Phys. Earth Planet. Inter.*, *119*, 237-257, https://doi.org/10.1016/S0031-9201(00)00134-5.
Bahr, K. and Simpson, F. (2002). Electrical anisotropy below slow- and fast-moving plates: palaeoflow in the upper mantle? *Science*, *295*, 1270-1272, https://doi.org/10.1126/science.1066161.
Beamish, D., T.D.G. Clark, E. Clarke and A.W.P. Thomson (2002). Geomagnetically induced currents in the UK: geomagnetic variations and surface electric fields. *J. Atmos. Sol.-Terr. Phys.*, *64*, 1779-1792, https://doi.org/10.1016/S1364-6826(02)00127-X.
Bolduc, L. (2002). GIC observations and studies in the Hydro- Québec power system. *J. Atmos. Solar-Terr. Phys.*, *64*, 1793-1802, https://doi.org/10.1016/51364-6826(02)00128-1.
Cagniard, L. (1953). Basic theory of the magnetotelluric method of geophysical prospecting. *Geophysics*, *15*, 123-157.
Cannon, P., M. Angling, L. Barclay, C. Curry, C. Dyer, R. Edwards, G. Green, M. Hapgood, R.B. Horne, D. Jackson, C. N. Mitchell, J. Owen, A. Richards, C. Rogers, K. Ryden, S. Saunders, M. Sweeting, R. Tanner, A. Thomson and C. Underwood (2013). *Extreme space weather impacts on engineered systems and infrastructure*. UK Royal Academy of Engineering, London, pp. 69, ISBN: 1-903496-95-0.
Chapman, S. and Ferraro, V. (1931). A new theory of magnetic storms. *Terr. Mag. 36*, 77-97. https://doi.org/10.1029/TE036i003p00171.
Cherevatova, M., Smirnov, M., Korja, T., Kaikkonen. P., Pedersen, L. B., Hübert, J. and Kalscheuer, T. (2014) Crustal structure beneath southern Norway imaged by magnetotelluric, *Tectonophysics*, *628*, 55-70, https://doi.org/10.1016/j.tecto.2014.04.036
Daglis, I. A., Thorne, R. M., Baumjohann, W. and Orsini, S. (1999). The terrestrial ring current: origin, formation and decay. *Reviews of Geophysics*, *37*, 407-438, https://doi.org/10.1029/1999RG900009.
Dong B., Wang Z.-Z., Liu L.-G., Liu L.-P., Liu C.-M., 2015. The proximity effect on the induced geoelectric field at the interface of different conductivity structures with lateral variations during geomagnetic storms. *Chinese J. Geophys.*, *58*(*1*): 238-246, https://doi.org/10.6038/cjg20150121.
Egbert, G. D. and Booker, J. R. (1986). Robust estimation of geomagnetic transfer functions. *Geophys. J. R. Astr. Soc.*, *87*, 173-194, https://doi.org/10.1111/j.1365-246X.1986.tb04552.x.
Engels, M., Korja, T. and Bear Working Group (2002). Multi sheet modelling of the electrical conductivity structure in the Fennoscandian Shield. *Earth, Planets and Space*, *54*, 559–573, https://doi.org/10.1186/BF03353045.
Gauss, C. F. (1839). Erläuterungen zu den Terminzeichnungen und den Beobachtungszahlen (Explanation of the drawings and measurements). In *Resultate aus den Beobachtungen des*

magnetischen Vereins im Jahre 1838 (Results from Observations of the Magnetism Society in 1838), eds. C. F. Gauss and W. Weber, Göttingen, Dieterichsche Buchhandlung, pp. 1-57.
Haak, V. and Hutton, V. R. S. (1986). Electrical resistivity in continental lower crust. In *The Nature of the Lower Continental Crust*, eds. J. B. Dawson, D. A. Carswell, J. Hall and K. H. Wedepohl, *Geol. Soc. Special Publication, 24*, 35-49, Blackwell Scientific Publications, Oxford, ISBN: 0632015616.
Hanekop, O. and F. Simpson (2006). Error propagation in electromagnetic transfer functions: what role for the magnetotelluric method in detecting earthquake precursors? *Geophys. J. Int.*, 165, 763-774, https://doi.org/10.1111/j.1365-246X.2006.02948.x.
Ivannikova, E., M. Kruglyakov, A. Kuvshinov, L. Rastätter and A.A. Pulkkinen (2018). Regional 3-D modeling of ground electromagnetic field due to realistic geomagnetic disturbances. *Space Weather, 16*, 476-500, https://doi.org/10.1002/2017SW001793.
Jaupart, C., Mareschal, J. C., Guillou-Frottier, L., Devaille, A. (1998). Heat flow and the thickness of the lithosphere in the Canadian Shield. *J. Geophys. Res., 103*, 15269-15286, https://doi.org/10.1029/98JB01395.
Kelbert, A., G. D. Egbert, and C. deGroot-Hedlin (2012). Crust and upper mantle electrical conductivity beneath the Yellowstone Hotspot Track, *Geology*, *40*, 447–450, https://doi.org/10.1130/G32655.1.
Kelbert, A., Balch, C. C., Pulkkinen, A., Egbert, G. D., Love, J. J., Rigler, E. J., & Fujii, I. (2017). Methodology for time-domain estimation of storm time geoelectric fields using the 3-D magnetotelluric response tensors. *Space Weather*, *15*, 874-894, https://doi.org/10.1002/2017SW001594.
Korja, T., Engels, M., Zhamaletdinov, A. A., Kovtun, A. A., Palshin, N. A., Smirnov, M. Y. (2002). Crustal conductivity in Fennoscandia—A compilation of a database on crustal conductance in the Fennoscandian Shield. *Earth, Planets and Space*, *54*, 535–558. https://doi.org/10.1186/BF03353044.
Lines, L. R. and Jones, F. W. (1973). The perturbation of alternating geomagnetic fields by three-dimensional island structures. *Geophys. J. R. astr. Soc., 32*, 133-154, 1973, https://doi.org.10.1111/j.1365-246X.1973.tb06524.x.
Liu L.-G., Liu C.-M., Zhang B., Wang Z-Z., Xiao X.-N., Han L.-Z. 2008. Strong magnetic storm's influence on China's Guangdong power grid. *Chinese J. Geophys*., *51*(*4*): 976-981, https://doi.org/10.1002/cjg2.1261.
Love, J., Pulkinnen, A., Bedrosian, P., Jonas, S., Kelbert, A., Rigler, E. J., Finn, C., Balch, C. C., Rutledge, R., Waggel, R. M., Sabata, A. T., Kozyra, J. U., Black, C. E. (2016). Geoelectric hazard maps for the continental United States. *Geophys. Res. Lett.*, *43*, 9415-9424, https://doi.org/10.1002/2016GL070469
Lucas, G., J.J. Love, A. Kelbert, P. A. Bedrosian and E. J. Rigler (2020). A 100-year geoelectric hazard analysis for the U.S. high-voltage power grid. *Space Weather*, *18*, e2019SW002329, https://doi.org/10.1029/2019SW002329
Oreskes, N., Schrader-Frechette, K. and Belitz, K. (1994). Verification, validation and confirmation of numerical models in the Earth sciences. *Science, 263*, 641-646, https://doi.org/10.1126/science.263.5147.641.
Osipova, I. L., Hjelt, S.-E. and Vanyan, L. L. (1989). Source field problems in northern parts of the Baltic Shield. *Phys. Earth Planet. Inter.*, *53*, 337-342, https://doi.org/10.1016/0031-9201(89)90019-8.
Parkinson, W. D. and Jones, F. W. (1979). The geomagnetic coast effect, *Rev. Geophys., 17*, 1999–2015, https://doi.org/10.1029/RG017i008p01999.
Radasky, W. A. (2011). Overview of the impact of intense geomagnetic storms on the US high voltage power grid. IEEE International Symposium on Electromagnetic Compatibility,

300-305, *IEEE Conference Publications*, New York, https://doi.org/10.1109/ISEM.2011.6038326.
Rasmussen, T. M., Roberts, R. G. and Pedersen, L. B. (1987). Magnetotellurics along the Fennoscandian long range profile. *Geophysical Journal*, *89*, 799–820, https://doi.org/10.1111/j.1365-246X.1987.tb05195.x.
Rosenqvist, L. and Hall, O. (2019). Regional 3-D Modeling and Verification of geomagnetically induced currents in Sweden. *Space Weather, 17*, 27-36, https://doi.org/10.1029/2018SW002084.
Sakkas, V., Meju, M., Khan, M. A., Haak, V., Simpson, F. (2002). Magnetotelluric images of the crustal structure of the Chyulu Hills volcanic field, Kenya. *Tectonophysics*, 346, 3-4, 169-185. https://doi.org/10.1016/S0040-1951(01)00276-1.
Schmucker, U. (1970). Anomalies of geomagnetic variations in the Southwestern United States. *Bull Scripps Inst. Ocean., University of California*, *13*, University of California Press Ltd, London, UK, pp 165, https://doi.org/10.1016/0031-9201(73)90061-7.
Schmucker, U. (1973). Regional induction studies: a review of methods and results. *Phys. Earth Planet. Inter.*, *7*, 365-378, https://doi.org/10.1016/0031-9201(73)90061-7.
Schultz, A. (2009), EMSCOPE: A continental scale magnetotelluric observatory and data discovery resource, *Data Sci. J.*, 8, P IGY6-IGY20, https://doi.org/10.2481/dsj.GG_IGY-009.
Schuster, A. (1889). The diurnal variation of terrestrial magnetism. *Phil. Trans. Roy. Soc. London, A210*, 467-518, https://doi.org/10.1098/rsta.1889.0015.
Simpson, F., Haak, V., Khan, M. A., Sakkas, V., Meju, M. (1997). The KRISP-94 magnetotelluric survey of early 1995: first results, *Tectonophysics*, 278, 261-271, https://doi.org/10.1016/S0040-1951(97)00107-8.
Simpson, F. (1999). Stress and seismicity in the lower continental crust: a challenge to simple ductility and implications for electrical conductivity mechanisms, *Surv. Geophys.*, *20*, 201-227, https://doi.org/10.1023/A:1006641922180.
Simpson, F. (2000). A three-dimensional electromagnetic model of the southern Kenya Rift: departure from two-dimensionality as a possible consequence of a rotating stress field. *J. Geophys. Res.*, *105*, 19321-19334, https://doi.org/10.1029/2000JB900106.
Simpson, F. (2002). A comparison of electromagnetic distortion and resolution of upper mantle conductivities beneath continental Europe and the Mediterranean using islands as windows. *Phys. Earth Planet. Inter.*, *129*, 117-130, https://doi.org/10.1016/S0031-9201(01)00264-3.
Simpson, F. and Bahr, K. (2005). *Practical Magnetotellurics*, Cambridge University Press, London, UK, pp. 254, https://doi.org/10.1017/CBO9780511614095.
Simpson, F. (2013). Distribution functions for anisotropic electrical resistivities due to hydrogen diffusivity in aligned peridotite and their application to the lithosphere-asthenosphere boundary, *Tectonophysics*, *592*, 31-38, https://doi.org/10.1016/j.tecto.2013.02.007.
Simpson, F. and Bahr, K. (2020a). Nowcasting and validating Earth's electric field response to extreme space weather events using magnetotelluric data: application to the September 2017 geomagnetic storm and comparison to observed and modelled fields in Scotland, *Space Weather*, 18, e2019SW002432, https://doi.org/10.1029/2019SW002432.
Simpson, F. and Bahr, K. (2020b). Estimating the electric field response to the Halloween 2003 and September 2017 magnetic storms across Scotland using observed geomagnetic fields, magnetotelluric impedances and perturbation tensors, *JSWSC*, swsc200019, https://doi.org/10.1051/swsc/2020049.
Simpson, F. and Warner, M. (1998). Coincident magnetotelluric, P-wave and S-wave images of the deep continental crust beneath the Weardale granite, NE England: seismic layering,

low conductance and implications against the fluids paradigm. *Geophys. J. Int.*, *133*, 419-434, https://doi.org/10.1046/j.1365-246X.1998.00512.x.
Siripunvaraporn W., Egbert, G., Lenbury, Y. and Uyeshima, M. (2005). Three-dimensional magnetotelluric: data space method, *Physics of the Earth and Planetary Interiors*, *150*, 3-14, https://doi.org/10.1016/j.pepi.2004.08.023.
Thomson, A.W.P., A. J. McKay, E. Clarke, and S. J. Reay (2005). Surface electric fields and Geomagnetically Induced Currents in the Scottish Power grid during the 30 October 2003 geomagnetic storm, *Space Weather*, **3**, S11002, https://doi.org/10.1029/2005SW000156.
Viljanen, A. H., Nevanlinna, K., Pajunpää, K. and Pulkkinen, A. (2001). Time derivative of the horizontal geomagnetic field as an activity indicator. *Ann. Geophys.*, *19*, 1107-1118, https://doi.org/10.5194/angeo-19-1107-2001.
Wait, J. R. (1954). On the relation between telluric currents and the Earth's magnetic field. Geophysics, 19, 281-289, https://doi.org/10.1190/1.1437994**.**
Watermann, J. and Gleisner, H. (2009). Geomagnetic variations and their time derivatives during magnetic storms at different levels of intensity. *Acta Geophysica*, *59*, 197-208, https://doi.org/10.2478/s11600-008-0045-7.
Weidelt, P. (1972). The inverse problem of geomagnetic induction. *Z. Geophys.*, *38*, 257-289.
Yang, B., Egbert, G. D., Kelbert, A. and Meqbel, N. M. (2015). Three-dimensional electrical resistivity of the north-central USA from EarthScope long period magnetotelluric data *Earth Planet. Sci. Lett.*, **422**, 87-93, https://doi.org/10.1016/j.epsl.2015.04.006.
Wik, M., Pirjola, R., Lundstedt, H., Viljanen, A., Wintoft, P. and Pulkkinen, A. (2009). Space weather events in July 1982 and October 2003 and the effects of geomagnetically induced currents on Swedish technical systems, *Annales Geophysicae*, *27*, 1775-1787, https://doi.org/10.5194/angeo-27-1775-2009.

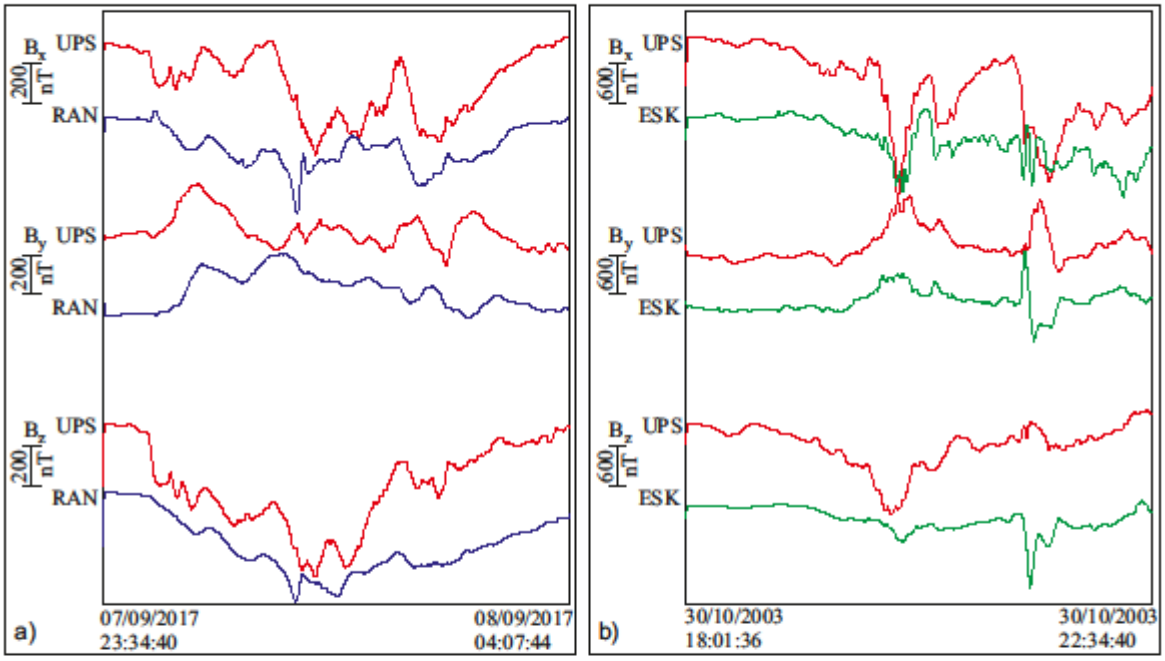

Figure 1 a) Measured magnetic field variations in north-south (B_x), east-west (B_y) and vertical (B_z) directions at a) RAN (blue traces) and UPS (red traces) during the 8th September 2017 magnetic storm and b) at ESK (green traces) and UPS (red traces) during the 30th October 2003 "Halloween" storm (30th October 2003).

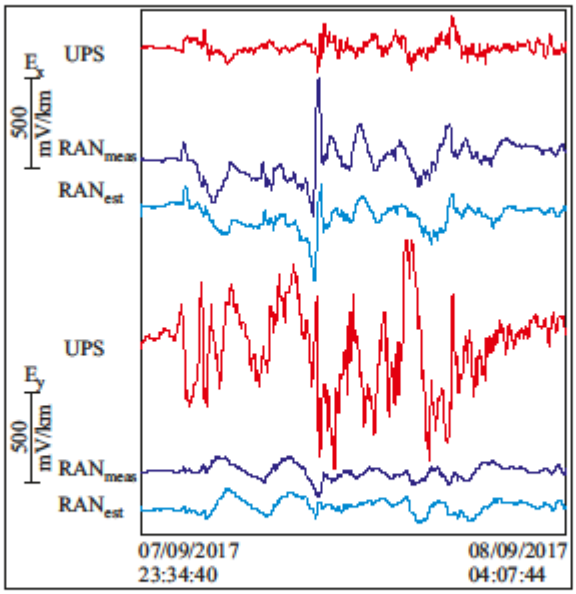

Figure 2 Comparison of measured (RAN_{meas} – dark blue trace) and estimated (RAN_{est} – light blue trace; UPS – red trace) north-south (E_x) and east-west (E_y) oriented electric fields at sites in Scotland (RAN) and Sweden (UPS) for the 8th September 2017 magnetic storm.

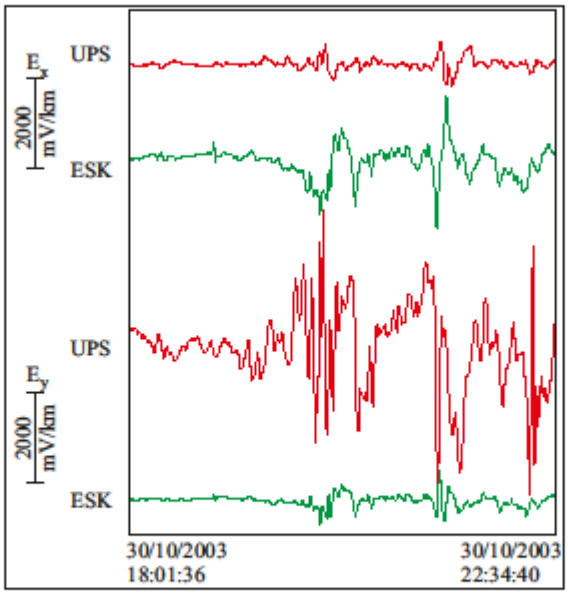

Figure 3 Electric fields estimated using magnetic field spectra (Figure 4) and MT impedance tensors at ESK (green traces) and UPS (red traces) during the 30th October "Halloween" storm.

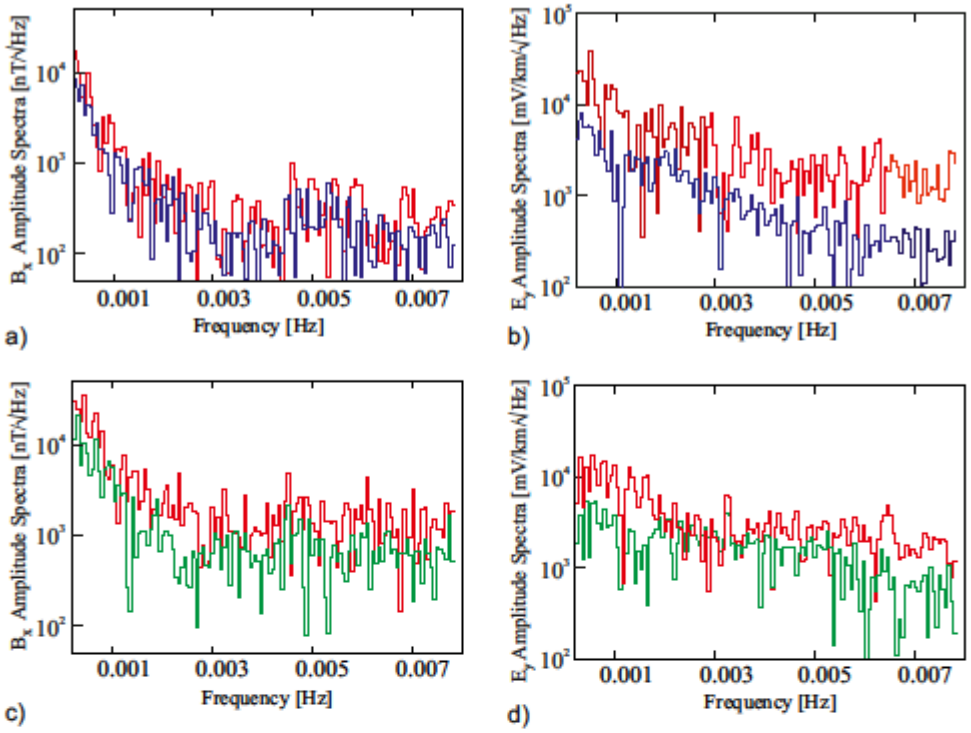

Figure 4 Amplitude spectra for the time windows shown in Figures 1-3: a) north-south magnetic (B_x) and b) east-west electric field (E_y) component of the 8th September 2017 magnetic storm measured at RAN (blue traces) and UPS (red traces); c) B_x component and d) E_y component of the 30th October 2003 "Halloween" storm on 30th October 2003 at ESK (green traces) and UPS (red traces). There is a steep increase in magnetic spectral amplitude at long periods.

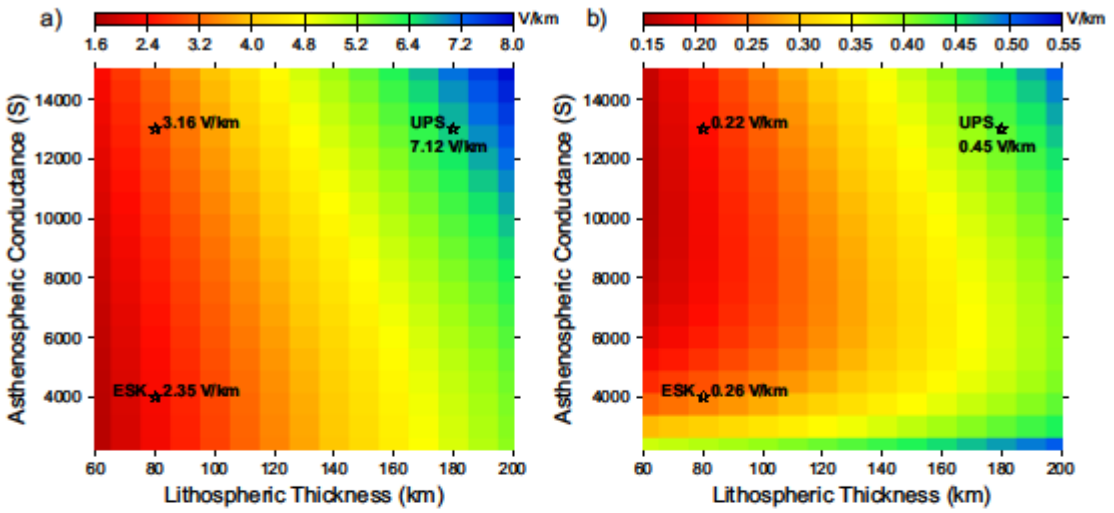

Figure 5 Electric-field magnitude as a function of lithosphere thickness and asthenosphere conductance at periods of a) 225 s, b) 3600 s calculated from equation 6 (Section 2.3, Methods). We assumed a value for τ_0 of 13 000 S – the maximum conductance of the asthenosphere below Sweden – because B_x at UPS is approximately twice as large as at ESK (see Section 2.1, Methods).